IEEE Journal of Microwaves

Received 24 January 2024; revised 23 April 2024; accepted 20 May 2024.
Date of current version 12 July 2024.

Digital Object Identifier 10.1109/JMW.2024.3405348

Arbitrary-Order Output Intercept Points of an Analog Receive Beamforming System

MATTHEW J. MONDICH [1], FRANK BUCHOLTZ [2], JOSEPH M. SINGLEY [1], AND KEITH J. WILLIAMS [1] (Member, IEEE)

(Regular Paper)

[1]Photonics Technology Branch, Optical Sciences Division, U.S. Naval Research Laboratory, Washington, DC 20375 USA
[2]Jacobs Technology, Inc., Herndon, VA 20171 USA

CORRESPONDING AUTHOR: Matthew J. Mondich (e-mail: matthew.j.mondich.civ@us.navy.mil).

This work was supported by the Office of Naval Research under an NRL 6.2 Base Program.

ABSTRACT We derive a general expression for the *m*th-order intercept point (*IPm*) of an analog RF receive beamforming system comprising multiple inputs, an array of nonlinear elements, and a single output. Given parallel inputs, the general *IPm* expression includes the gain and nonlinearity of each element in the array as well as both intrinsic and extrinsic loss factors and phase shifts. We then impose constraints on the calculation of *IPm* by making certain assumptions about the statistical relationship between the phases of the distortion signals at the output to obtain the coherent and incoherent *m*th-order output intercept points (*OIPm*), which determine lower and upper bounds, respectively, on an actual measured output intercept point. Finally, we present the results of a series of experiments and show that the *OIP2* and *OIP3* obtained from 36 independent measurements all fall between the theoretical calculated bounds. These results will be of utility in the design, analysis, and testing of analog phased-arrays, multi-channel receivers, and receive-mode beamformers.

INDEX TERMS Analog beamforming, distortion, intercept point, multi-channel receivers, output intercept point, parallel inputs, phased-arrays, receive-mode beamformers.

I. INTRODUCTION

Many modern-day radar and telecommunications applications utilize beamforming that is performed in the digital domain. Digital beamforming offers great flexibility and control [1], [2], [3], thereby enabling beam-steering to any desired angle. Furthermore, signal processing techniques such as predistortion and nonlinear equalization that minimize system nonlinearity and in turn extend the dynamic range [2] can be performed very efficiently in the digital domain. However, digital beamforming systems have certain drawbacks such as the inability to provide spatial filtering on receive to mitigate strong interferers in a dense signal environment [1], [4] and high power consumption due to the analog-to-digital and digital-to-analog converters [3].

In contrast, analog beamforming systems offer clear advantages for certain applications, especially those where compactness [5], low power consumption [3], simplicity [3], or wide bandwidths [3], [5] are needed. Recently analog approaches have been considered for multifunction wideband antenna systems for joint electronic warfare/radar electronically-steered arrays [6]. In these applications, a small amount of noise figure can be traded off for maximizing dynamic range where intermodulation products clutter the spectrum. This is especially useful for systems that experience high co-site interference or that put a premium on wide bandwidth detection and signal sorting. In addition to military needs, analog beamforming can also be advantageous for some 5G applications [3], [5] where simplicity and power efficiency are benefits while trading off adaptability and reconfigurability. In general, certain systems can benefit from keeping signals in the analog domain before eventual transition to the digital domain. These benefits include near-instantaneous beamforming with moderate angular rejection or out-of-band rejection that are important in such applications as amplitude-based direction finding, main-beam power gain, and retro-directive beamforming.

Both high dynamic range and high linearity are needed in these applications where the analog receive beamformer

(ARBF) must operate in a complex electromagnetic environment and be subjected to multiple simultaneous signals. Therefore, quantifying the nonlinear behavior of such a system is important. The intercept point formulas for single-input, single-output devices and serial cascades are well known [7], [8], [9], [10]. These formulas are not applicable to multiple-input, single-output systems, such as an ARBF system, comprising a parallel array of channels each containing a serial cascade of nonlinear devices. Thus, there is a need for an analysis approach for ARBF systems. Importantly, distinguishing the assumptions of coherence versus incoherence among distortion signals sets lower (worst case) and upper (best case) bounds, respectively, on the nonlinear behavior of a system, as will be described in detail below.

Previous works on ARBF systems were limited in that they a) contain analyses that are restricted to coherent in-phase distortion signals, or b) consider only second- and third-order nonlinearity, or c) contain no nonlinearity analysis at all. Rupakula et al. [11] derived third-order input intercept points (*IIP3*) for receive-mode 5G arrays containing multiple nonlinear elements in series on parallel channels but did not consider any other nonlinearity order and did not consider partially-incoherent addition of the distortion signals. Gatti et al. [12] derived *IIP3* equations for an active array antenna with a receiver comprising a parallel array of channels, but only where each channel comprised a single nonlinear element. No other nonlinearity orders were considered nor was the case of incoherent distortion signals. Holzman [13] derived *m*th-order output intercept points (*OIPm*) of an active phased array antenna but likewise only considered the case of each channel containing a single nonlinear element and did not consider the case of incoherent distortion signals. Recently, Bucholtz et al. [14] derived the worst-case *OIP2* and *OIP3* as well as the overall gain and the third-order spurious-free dynamic range of an ARBF system using a power-series nonlinearity model but did not consider the case of incoherent distortion signals. Navarrini et al. [15] and Chen et al. [16] designed, fabricated, and tested multi-channel receivers but did not analyze their nonlinearity. Spoof et al. [17] and Mondich et al. [18] derived noise figure equations for hybrid analog/digital and photonic receive-mode beamforming systems, respectively, but did not treat nonlinearity.

Hence, the goal of this work is to derive arbitrary-order output intercept point equations for quantifying the nonlinear behavior of ARBF systems. These include the general expressions to arbitrary nonlinearity order for the actual output intercept point, and the corresponding theoretical lower and upper bound output intercept points. Typically the lower (worst case) bound of the intercept point is of most practical interest. However, the most general expression for the intercept point, one that contains *all* the relevant RF parameters, can be of practical utility at the design phase where decisions on how to allocate various components must be made while optimizing performance. In addition, the theoretical lower and upper bounds have practical utility as a check on system measurement since any actual measurement of an intercept point must fall in between these theoretical bounds.

The remainder of the paper is organized as follows. In Section II we provide a brief review of the well-known output intercept point approach for analyzing nonlinear RF behavior and we lay the groundwork for analyzing an ARBF array. In Section III we derive the general *m*th-order intercept point (*IPm*) expression for the full ARBF system written in terms of all the relevant system parameters. In this section we also obtain *OIPm* expressions for the coherent and incoherent cases and show that for a single channel these expressions reduce to the well-known serial cascade equations. In Section IV we evaluate the ARBF system *OIPm* expressions for $m = 3$ and consider the special cases of purely parallel and purely serial arrays. We obtain expressions and plots for cases where a) all the nonlinear elements in the array are identical, and b) where all elements except one are identical. Case (a) is helpful in understanding how *OIP3* scales with array size while case (b) quantifies the effect of one "bad" element on array performance, where the "bad" element has low *OIP3* and gain. In Section V we present experimental results for a 2 x 2 ARBF system comprising two channels each containing two nonlinear elements and show that, for 36 independent measurements of *OIPm* ($m = 2, 3$), *all* the results fall within the theoretical calculated bounds given by the coherent and incoherent expressions. Section VI is a summary and short discussion of the results. Appendix I provides a glossary and description of the large number of parameters that appear in the general expressions. Appendix II lists some mathematical identities that are useful in Sections III and IV. Appendix III includes tables of experimental parameters corresponding to the experimental results in Section V.

These results will be of practical use in the design, analysis, and testing of analog phased-arrays, multi-channel receivers, and receive-mode beamformers.

II. BACKGROUND

In this section we review briefly the standard approach to evaluating intercept points for a single nonlinear device and for a single serial cascade of devices to establish nomenclature and to define symbols.

Parameters and methods for quantifying the nonlinear behavior of RF devices comprising a single input and single output are well-known and well-accepted by the RF community. Useful among these parameters is the *m*th-order output intercept point *OIPm*, obtained experimentally with the use of a diagram such as the one shown in Fig. 1. Here, for a defined RF input voltage, the output powers at a fundamental frequency and an *m*th-order distortion frequency are together plotted in the small-signal regime, the data plots are extrapolated to higher power levels, and the point at which the two plots intersect is defined as the *OIPm* of the device.

The same analysis can be applied to a single-input, single-output system, such as a serial cascade of nonlinear elements (NLEs), or stages, as shown in Fig. 2(a), to obtain the actual, end-to-end *OIPm* of the array. In this case, the possibility

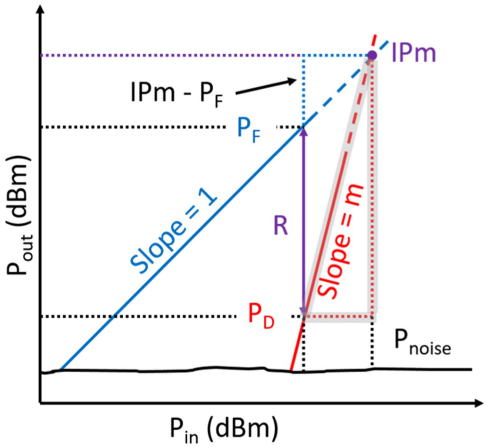

FIGURE 1. Output power, P_{out}, versus input power, P_{in}. P_F: extrapolated small-signal output power of fundamental; P_D: extrapolated small-signal output power of mth-order distortion; R: relative suppression between P_F and P_D; P_{noise}: output noise power.

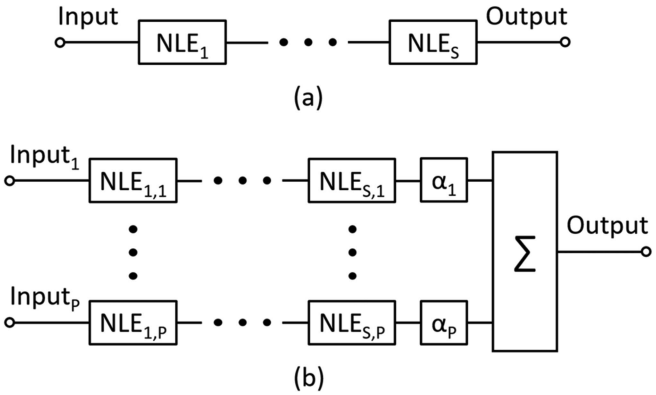

FIGURE 2. (a) Single-input, single-output serial cascade of S nonlinear elements (NLEs) or stages. (b) Analog receive beamforming (ARBF) system comprising S NLEs in series on P parallel channels. The P parallel channel inputs are combined in a perfectly linear summing junction, denoted by Σ, to produce a single output. α_p is an amplitude weighting factor that accounts for intentionally applied weighting and the loss due to the amplitude coupling coefficient associated with the employed signal combination technique.

arises to *predict* the end-to-end *OIPm* in terms of the *OIPm* values of the individual components. If the RF properties, including device phase shifts and inter-element delays and losses are all known, then the calculation of the output intercept point is relatively straightforward. However, the output intercept point calculated in this fashion may not be "the *OIPm*" as commonly accepted by the RF community. We call the calculation containing the phase shifts the "*IPm*" to avoid any confusion with "the *OIPm*," which is based on assumptions about the phase shifts and therefore does not explicitly contain any phase terms. To conform to industry standards, calculation of *OIPm* for a serial cascade implies that a significant assumption has been made, namely, that at the output the distortion signals—one from each device—are completely coherent and are all exactly in phase. This assumption yields the largest total distortion signal at the output and, hence, the minimum or most pessimistic estimate of *OIPm* [7], [8], [9], [10]. It is this most-conservative, coherent estimate that is universally assumed when the *OIPm* of a serial cascade is calculated in terms of the properties of the individual NLEs.

Also in use are two less common alternative assumptions about the phases of the distortion signals. In one, the phases of the distortion signals are assumed to be completely incoherent [7]. This assumption gives rise to an estimate of *OIPm* that is always larger than the in-phase coherent estimate. (The other, perhaps least-common and least-used assumption is that the distortion signals are coherent but all combine destructively, that is, exactly out of phase [8]. However, this approach is difficult to implement for systems comprising more than two elements.) In an actual system, it is likely that the distortion signals will be neither perfectly in phase nor perfectly incoherent. Hence, the value of any actual measured intercept point will lie in between the calculated minimum (coherent) and maximum (incoherent) values. Note that although the output of a serial cascade of, say, S elements contains the vector sum of S individual distortion signals, it contains only one signal at a fundamental frequency. Since only the total output power at a particular frequency is relevant, the phase of this single fundamental signal is of no consequence and, therefore, the terms coherent and incoherent will refer only to the phases of the distortion signals.

Consider now the ARBF system of Fig. 2(b), comprising P parallel input channels, each containing S nonlinear elements in series for a total of SP nonlinear elements. Here the output consists of SP distortion signals and P fundamental signals and so, in this case, the relative phases of the fundamental signals at the single output must also be taken into account.

In this work we obtain expressions for the *IPm* and *OIPm* of the full ARBF system shown in Fig. 2(b) assuming that the RF power gain and *OIPm* are known for each individual device, along with the loss between devices, the coupling and excess losses of the combiner, and any intentional channel weighting. We make three different sets of assumptions regarding relative RF phases at the output:

1) no global assumption regarding any output phases;
2) the fundamental signals are all coherent and exactly in phase and the distortion signals are all coherent and exactly in phase;
3) the fundamental signals are all coherent and exactly in phase but the distortion signals are all completely incoherent.

In order for the *IPm* expression resulting from the first set of assumptions to be utilized it is necessary that all the relative phase differences be known *a priori* and, hence, this expression will be of utility in a design phase. The second assumption, the coherent assumption, conforms to the industry-standard, worst-case estimate of *OIPm* and gives the lower bound. The third assumption, the incoherent case, provides the upper bound on the overall *OIPm*.

Before proceeding we clarify our use of the terms coherent and incoherent. Let $\Delta\phi$ denote the phase difference between two RF signals and consider the temporal average $\langle \cos \Delta\phi \rangle$. Consider first the case where the phase difference $\Delta\phi$ is fixed for all time. Then the two signals are said to be *coherent*

and $\langle \cos \Delta\phi \rangle = \cos \Delta\phi$ can take any value between -1 and $+1$, including zero, depending on the value of $\Delta\phi$. On the other hand, if there is no fixed phase relationship between the signals then the phase difference becomes a random variable. In this case the average $\langle \cos \Delta\phi \rangle$ can still take any value between -1 and $+1$ depending on the probability distribution of the random variable. In the special case where the phase difference is uniformly distributed over the range $[0,\ 2\pi)$ then $\langle \cos \Delta\phi \rangle = 0$. In this particular case the signals are said to be *incoherent*. In all other cases the signals are said to be *partially coherent*. Hence, the value of $\langle \cos \Delta\phi \rangle$ alone does not determine coherence or incoherence. (For example, $\langle \cos \Delta\phi \rangle = 0$ occurs when the signals are either a) completely coherent but with $\Delta\phi = \pi/2$ or b) completely incoherent.) Instead, it is the probability distribution of the random variable $\Delta\phi$ that determines the coherence relationship between the two signals. For the analysis presented here we assume that $\Delta\phi$ is uniformly distributed when we consider the incoherent case.

In an actual system, the distortion signals will likely be partially coherent since the noise in any NLE will likely be uncorrelated to the noise in any other NLE. Hence, any actual measurement of the output intercept point must lie between the bounds set by the two extreme assumptions among the distortion voltages: coherence (worst case) and incoherence (best case). The 36 independent experimental measurements reported in Section V are all consistent with this assertion.

Recall that *IPm* denotes the output power at which the fundamental and *m*th-order distortion powers are equal. As noted above, a particular constraint must be imposed on the phases of the distortion signals for *IPm* to represent *OIPm* in the case of a serial cascade or ARBF system. In the derivation of *IPm*, it will be assumed that the input voltage to the device or system comprises two small-signal, equal-amplitude, closely-spaced, incommensurate RF tones.

Let m represent the slope of the hypotenuse of the triangle drawn with heavy-shaded sides in Fig. 1. From the ratio of the change in P_{out} *(dBm)* to the change in P_{in} *(dBm)* for the same triangle we have

$$m = \frac{R\,(dB) + IPm\,(dBm) - P_F\,(dBm)}{IPm\,(dBm) - P_F\,(dBm)}, \tag{1}$$

where the relative suppression R between the extrapolated small-signal fundamental and distortion output powers, P_F and P_D, respectively, is $R = P_F - P_D$. From (1), we obtain

$$IPm\,(dBm) = \frac{R\,(dB)}{m-1} + P_F\,(dBm)\,, \tag{2}$$

which can be expressed in power as

$$IPm = r^{1/(m-1)} p_F\,, \tag{3}$$

where $r = p_F/p_D$, and p_F and p_D are powers measured in linear units (W). Inserting r into (3) and rearranging yields

$$\frac{1}{IPm^{(m-1)}} = (2Z_0)^{(m-1)} \left(\frac{V_D}{V_F^m}\right)^2, \tag{4}$$

where V_F and V_D are the output voltage amplitudes of the fundamental and the *m*th-order distortion, respectively, and Z_0 is the real part of the output load impedance (resistance), which is assumed to be matched to the source, to the NLE input, and to the NLE output. Equation (4) is the general *IPm* equation that will be applied to an ARBF system.

Noting that $IPm = OIPm$ for a single NLE with one input and one output and using (4), the *OIPm* is

$$OIPm = \frac{V_F^{2m/(m-1)}}{2Z_0 V_D^{2/(m-1)}}. \tag{5}$$

Subsequent analysis will make use of (5).

Our approach is as follows.

1) We first define the architecture of the analog array in terms of P parallel channels each containing S NLEs.
2) We next derive the actual (no phase assumptions) intercept point *IPm* for nonlinear order m by summing the linear voltages and the distortion voltages from each NLE where each voltage is represented in phasor form. This gives rise to a somewhat unwieldy expression comprising dozens of parameters to account for all the relevant voltages and phases in the system. A complete list of the parameters is found in Appendix I along with explanatory two figures.
3) In order to obtain the bounds we next invoke the assumptions of 1) coherent distortion signals all exactly in phase (lower bound), and 2) incoherent distortion signals (upper bound).
4) We next evaluate both the coherent and incoherent bounds for $m = 3$ in the simple limiting case of a parallel array with a single NLE on each channel (Section IV-A).
5) Finally, we consider cases for $m = 3$ where one NLE in the entire array is "bad" and evaluate the effect of the position of this one "bad" NLE on the output intercept point of the system for both the coherent and incoherent bounds (Sections IV-B–IV-D).

III. ARBF SYSTEM

In this section we derive the general expression for the *m*th-order intercept point *IPm* of the analog receive beamforming system shown in Fig. 2(b), from which we obtain the coherent (worst case) and incoherent (best case) *OIPm* expressions.

Appendix I contains a complete list of all the parameters that are used in the analysis in this section along with their definitions and related figures. The reader may find the identities in Appendix II to be helpful in working through various details of the calculations.

A. IPm

The general expression for the *IPm* in (4) can be applied to an ARBF system with P parallel inputs, S elements in series on each of the P channels, and one output [Fig. 2(b)]. The output thus comprises the sum of SP distortion signals and P fundamental signals. To track the phases of signals as they propagate through the system all voltages will be represented

by complex phasors. Consequently, the voltages in (4) can be generalized to

$$V_D \rightarrow \sum_{s=1}^{S}\sum_{p=1}^{P} v_{D,sp} \tag{6}$$

and

$$V_F \rightarrow \sum_{p=1}^{P} v_{F,p}. \tag{7}$$

Here, $v_{D,sp}$ is the phasor representing the distortion voltage at the output that originated in the NLE at location s on channel p and $v_{F,p}$ is the phasor representing the fundamental voltage at the output from channel p. We have found it beneficial to treat the fundamental voltages in a manner analogous to the distortion voltages and, provided we account for the gains properly, we can write

$$v_{F,p} \rightarrow v_{F,sp} \tag{8}$$

for the fundamental voltage phasor at the output. With this modification, and since the order of summation does not matter, the single-input, single-output equation (4) becomes, for the ARBF system,

$$\begin{aligned}\frac{1}{IPm^{(m-1)}} &= \frac{p_{D,tot}}{p_{F,tot}^{m}} \\ &= (2Z_0)^{(m-1)}\left|\sum_{s=1}^{S}\frac{\sum_{p=1}^{P} v_{D,sp}}{\left(\left|\sum_{p=1}^{P} v_{F,sp}\right|^2\right)^{m/2}}\right|^2. \end{aligned}\tag{9}$$

We have taken the perhaps unusual approach of performing the sum over the p-index first followed by the sum over the s-index as shown diagrammatically in Fig. 3. With this approach, the expressions for the coherent and incoherent *OIPm* of the ARBF system can be written in a form analogous to that of the familiar equations for a serial cascade, which is shown in Section III-B.

At first glance, the expression on the second line of (9) may look incorrect since it appears to yield $S \times P$ fundamental voltages at the system output. However, upon insertion of $v_{F,sp}$ (defined in list of parameters in Appendix I) into (9), (9) gives P fundamental voltages at the system output, which is the correct result. The P fundamental voltages at the system output correspond to the P input voltages to the system, one per channel, where each channel input voltage has the same amplitude V_0.

In the analysis that follows, it will be assumed that the channels are phase matched between each of the inputs and reference plane o/p A over the operating frequency range of the system (see Fig. 15 in Appendix I) such that $\chi_p = \chi_p' - \chi_1' = 0$ and that all phase imbalances between channels occur between o/p A and the system output, which are accounted for by ψ_p and γ_p. Taking this approach will simplify the analysis by allowing the relative phases at the fundamental and distortion frequencies between channels p and 1 at the output to be treated the same way (i.e., with ψ_p and γ_p).

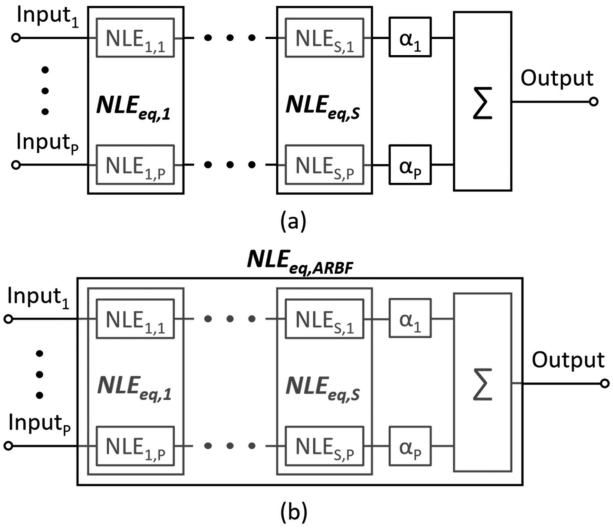

FIGURE 3. Reduction of ARBF system in Fig. 2(b) to (a) a serial cascade of S equivalent NLEs ($NLE_{eq,1}$ to $NLE_{eq,S}$) with P inputs and P outputs, where each input and output corresponds to the input and output of each of the P NLEs in $NLE_{eq,s}$, plus channel amplitude weighting factors and a summing junction; and (b) further reduction of (a) to a single equivalent NLE ($NLE_{eq,ARBF}$) with P inputs and one output.

Prior to deriving the *IPm* of the ARBF system, we first derive expressions for the distortion and fundamental output powers.

The total distortion power from all S stages and P channels at the system output is

$$\begin{aligned} p_{D,tot} &= \frac{1}{2Z_0}\left|\sum_{s=1}^{S}\sum_{p=1}^{P} v_{D,sp}\right|^2 \\ &= \frac{1}{2Z_0}\sum_{s=1}^{S}\left(\sum_{p=1}^{P} D_{sp}^2 + \sum_{p\neq q=1}^{P} D_{sp}D_{sq}\cos\xi_{sp,sq}\right) \\ &\quad + \frac{1}{2Z_0}\sum_{s\neq r=1}^{S}\left(\sum_{p=1}^{P} D_{sp}D_{rp}\cos\xi_{sp,rp}\right. \\ &\quad \left. + \sum_{p\neq q=1}^{P} D_{sp}D_{rq}\cos\xi_{sp,rq}\right). \end{aligned}\tag{10}$$

Equation (10) contains four sums resulting in a total of S^2P^2 distortion power terms at the system output: 1) a first sum with SP terms, where $s = r$ and $p = q$, which accounts for the distortion voltage from stage s on channel p mixing with itself; 2) a second sum with $S(P^2 - P)$ terms, where $s = r$ and $p \neq q$, which accounts for the distortion voltage from stage s on channel p mixing with the distortion voltage from stage s on channel q; 3) a third sum with $(S^2 - S)P$ terms, where $s \neq r$ and $p = q$, which accounts for the distortion voltage from stage s on channel p mixing with the distortion voltage from stage r on channel p; and 4) a fourth sum with $(S^2 - S)(P^2 - P)$ terms, where $s \neq r$ and $p \neq q$, which accounts for

the mixing of the distortion voltage from stage s on channel p with the distortion voltage from stage r on channel q.

The total fundamental power from all P channels at the system output, obtained by setting $\chi_p = 0$ for phase matched channels between inputs 1 to P and o/p A, is

$$p_{F,tot} = \frac{1}{2Z_0}\left|\sum_{p=1}^{P} v_{F,p}\right|^2 = \frac{1}{2Z_0}\left(\sum_{p=1}^{P} F_{Sp}^2 + \sum_{p\neq q=1}^{P} F_{Sp}F_{Sq}\cos\psi_{p,q}\right). \quad (11)$$

Equation (11) contains two sums yielding P^2 total fundamental power terms at the output of the system: 1) a first sum with P terms, where $p = q$, which accounts for the mixing of the fundamental voltage from channel p with itself; and 2) a second sum with $(P^2 - P)$ terms, where $p \neq q$, which accounts for the mixing of the fundamental voltages from channels p and q.

We can now obtain the general *IPm* of the ARBF system. From (9), (10), (11), and the definitions in Appendix I, we find

$$IPm = \frac{1}{2Z_0}\left[\sum_{s=1}^{S}\frac{\sum_{p=1}^{P} D_{sp}^2 + \sum_{p\neq q=1}^{P} D_{sp}D_{sq}\cos\xi_{sp,sq}}{\left(\sum_{p=1}^{P} F_{sp}^2 + \sum_{p\neq q=1}^{P} F_{sp}F_{sq}\cos\psi_{p,q}\right)^m} + \sum_{s\neq r=1}^{S}\frac{\sum_{p=1}^{P} D_{sp}D_{rp}\cos\xi_{sp,rp} + \sum_{p\neq q=1}^{P} D_{sp}D_{rq}\cos\xi_{sp,rq}}{\left(\sum_{p=1}^{P} F_{sp}F_{rp} + \sum_{p\neq q=1}^{P} F_{sp}F_{rq}\cos\psi_{p,q}\right)^m}\right]^{\frac{-1}{(m-1)}}. \quad (12)$$

Equation (12) is a general result that can be used to compute the *IPm* of an ARBF system if all of the system parameters are known. Recall that it is also useful to estimate the value of the intercept point by making certain global assumptions about the relative phases in (12).

We first assume the channels are phase matched over the operating frequency range of the system such that there is a zero-relative phase difference between channels at the output, that is, $\gamma_p = \gamma_q = 0$ and $\psi_p = \psi_q = 0$, hence, $\gamma_{p,q} = \psi_{p,q} = 0$. With this assumption (12) becomes

$$IPm = \frac{1}{2Z_0}\left[\sum_{s=1}^{S}\frac{\sum_{p=1}^{P} D_{sp}^2 + \sum_{p\neq q=1}^{P} D_{sp}D_{sq}\cos\varphi_{sp,sq}}{\left(\sum_{p=1}^{P} F_{sp}\right)^{2m}} + \sum_{s\neq r=1}^{S}\frac{\sum_{p=1}^{P} D_{sp}D_{rp}\cos\varphi_{sp,rp} + \sum_{p\neq q=1}^{P} D_{sp}D_{rq}\cos\varphi_{sp,rq}}{\left(\sum_{p=1}^{P} F_{sp}\right)^m\left(\sum_{p=1}^{P} F_{rp}\right)^m}\right]^{\frac{-1}{(m-1)}}. \quad (13)$$

Alternative global assumptions, the coherent and incoherent cases, are analyzed next. Note that, in these cases, we are justified in denoting the general *IPm* by the accepted definition of *OIPm*.

B. COHERENT & INCOHERENT OIPm

Since all the individual relative phase relationships in (13) are usually unknown in practice, we will make assumptions about the relative phases to predict the value of *OIPm*. The coherent *OIPm* corresponds to the case $\varphi_{sp,sq} = \varphi_{sp,rp} = \varphi_{sp,rq} = 0$, that is, when the distortion voltages from stages r and s on channels p and q are all mutually coherent and all combine perfectly in phase at the system output. This yields the lower bound or worst-case *OIPm* of the ARBF system. In contrast, the incoherent *OIPm* is obtained when $\varphi_{sp,sq}$, $\varphi_{sp,rp}$, and $\varphi_{sp,rq}$ are assumed to be mutually incoherent and uniformly distributed over $[0, 2\pi)$ such that all the average values $\langle\cos\varphi_{sp,sq}\rangle = \langle\cos\varphi_{sp,rp}\rangle = \langle\cos\varphi_{sp,rq}\rangle = 0$. This results in the upper bound or best-case *OIPm* of the ARBF system.

With these assumptions we find, for the coherent case,

$$OIPm_{coh} = \frac{1}{2Z_0}\left[\sum_{s=1}^{S}\frac{\sum_{p=1}^{P} D_{sp}}{\left(\sum_{p=1}^{P} F_{sp}\right)^m}\right]^{-2/(m-1)} \quad (14)$$

and, for the incoherent case,

$$OIPm_{incoh} = \frac{1}{2Z_0}\left[\sum_{s=1}^{S}\frac{\sum_{p=1}^{P} D_{sp}^2}{\left(\sum_{p=1}^{P} F_{sp}\right)^{2m}}\right]^{-1/(m-1)}. \quad (15)$$

These expressions can be expanded using $D_{sp} = V_{D,sp}\sqrt{g_{D,sp}}\alpha_p$, $F_{sp} = V_{F,sp}\sqrt{g_{F,sp}}\alpha_p$, and further simplified by making two additional assumptions: 1) the net linear power gains at the distortion (and fundamental) frequencies are the same on all channels, that is, $g_{D,sp} = g_{D,s}$ and $g_{F,sp} = g_{F,s}$; and 2) the distortion (and fundamental) voltage phasor amplitudes at the output of stage s are the same on all channels, that is, $V_{D,sp} = V_{D,s}$ and $V_{F,sp} = V_{F,s}$. Applying the two additional simplifying assumptions to (14) and (15) and using (5) yields

$$OIPm_{coh} = \left(\sum_{p=1}^{P}\alpha_p\right)^2\left(\sum_{s=1}^{S}\frac{g_{D,s}^{1/2}}{OIPm_s^{(m-1)/2}g_{F,s}^{m/2}}\right)^{-2/(m-1)} \quad (16)$$

and

$$OIPm_{incoh} = \frac{\left(\sum_{p=1}^{P}\alpha_p\right)^{\frac{2m}{(m-1)}}}{\left(\sum_{p=1}^{P}\alpha_p^2\right)^{\frac{1}{(m-1)}}}\left(\sum_{s=1}^{S}\frac{g_{D,s}}{OIPm_s^{(m-1)}g_{F,s}^m}\right)^{-1/(m-1)}. \quad (17)$$

Aside from the multiplicative factors containing the per-channel voltage amplitude weighting factors α_p, (16) and (17) are of the same form as the *OIPm* equations for a serial cascade obtained under the coherent and incoherent assumptions. With $P = \alpha_p = 1$ and $g_{D,s} = g_{F,s} = g_s = \prod_{z=s+1}^{S} G_z$, (16) and (17) reduce to the well-known serial cascade equations [7], [8], [9], [10].

TABLE 1. Scaling of the ARBF System *OIPm* With Channel Count *P* for Each Combiner Type

	Lossless Combiner	Wilkinson Combiner	Resistive Combiner
$OIPm_{coh}$	P^2	P	Independent of P
$OIPm_{incoh}$	$P^{(2m-1)/(m-1)}$	$P^{m/(m-1)}$	$P^{1/(m-1)}$

From (16) and (17) it is seen that the dependence of *OIPm* on channel count P depends on the nature of the signal combiner as shown in Table 1 assuming no intentionally applied weighting ($w_p = 1$) and identical channels. In practice, of course, the scaling of *OIPm* is limited by the power handling of the signal combiner and therefore does not grow without bound by simply adding more channels.

In the next section we consider the specific case $m = 3$ to provide further insight into the nonlinear behavior of an ARBF system.

IV. LIMITING CASES OF ARBF SYSTEM OIPm

Due to its importance and familiarity, in this section we evaluate *OIPm* for third-order intermodulation distortion using (14) and (15) as starting points. We also make the following simplifying assumptions:

1) The combiner is a Wilkinson-type device and there is no intentional weighting: $c_v = 1/\sqrt{P}$ and $w_p = 1$.
2) Inter-element losses are neglected: $L_{D,sp} = L_{F,sp} = 1$.
3) For any NLE, the RF power gains at the fundamental and distortion frequencies are equal: $G_{D,sp} = G_{F,sp} \equiv G_{sp} > 1$.

The identities in Appendix II are helpful in obtaining the following results.

A. PARALLEL ARRAY: S = 1; P = ARBITRARY; IDENTICAL ELEMENTS

Consider a parallel array of P identical NLEs. From (14) and (15), the coherent and incoherent *OIP3* are, respectively,

$$OIP3_{coh,ident} = P \cdot OIP3, \tag{18}$$

$$OIP3_{incoh,ident} = P^{3/2} \cdot OIP3. \tag{19}$$

The coherent *OIP3* of the parallel array is enhanced by a factor of P, whereas the incoherent *OIP3* is enhanced by a factor of $P^{3/2}$. Gatti [12], Holzman [13], and Bucholtz [14] also obtained the same factor of P improvement in *OIP3* for the coherent case.

B. PARALLEL ARRAY: S = 1; P = ARBITRARY; 1-BAD ELEMENT

We now consider a parallel array containing $(P-1)$ identical, "good" NLEs and one "bad" NLE with degraded gain and *OIP3*. The "good" NLEs have a power gain of G and a third-order output intercept point of *OIP3*. The "bad" NLE, located at $p = \rho$, has a reduced power gain of $\gamma \cdot G$, $(0 \le \gamma \le 1)$, and a reduced third-order output intercept point of $\chi \cdot OIP3$, $(0 \le \chi \le 1)$. The degradation in the *OIP3* of the parallel array due to one "bad" NLE can be quantified by the ratio of *OIP3* for all identical, "good" NLEs to *OIP3* for one "bad" NLE ($R_{1-bad} \ge 1$). Hence,

$$R_{1-bad,coh} \equiv \frac{OIP3_{coh,ident}}{OIP3_{coh,1-bad}} = \frac{P^2\left[(P-1)+\left(\frac{\gamma^{3/2}}{\chi}\right)\right]}{\left[(P-1)+\gamma^{1/2}\right]^3}, \tag{20}$$

$$R_{1-bad,incoh} \equiv \frac{OIP3_{incoh,ident}}{OIP3_{incoh,1-bad}} = \frac{P^{5/2}\left[(P-1)+\left(\frac{\gamma^3}{\chi^2}\right)\right]^{1/2}}{\left[(P-1)+\gamma^{1/2}\right]^3}. \tag{21}$$

Equations (20) and (21) are plotted in Figs. 4 and 5, respectively, for $S = 1$ and $P = 4$, 8, and 16. The following observations can be made: 1) the coherent case is somewhat more forgiving of one "bad" NLE; 2) the reduction is independent of the location ρ of the "bad" NLE; 3) the reduction is independent of the starting values of G and *OIP3*; and 4) the effect of the "bad" NLE decreases as P grows.

C. SERIAL ARRAY: S = ARBITRARY; P = 1; 1-BAD ELEMENT

A serial array comprising $(S-1)$ identical, "good" NLEs and one "bad" NLE is analyzed in this section. The "bad" NLE, located at $s = \sigma$, has a reduced power gain ($\gamma \cdot G$, $0 \le \gamma \le 1$) and reduced third-order output intercept point ($\chi \cdot OIP3$, $0 \le \chi \le 1$) compared to the other "good" NLEs in the array with power gain G and third-order output intercept point *OIP3*. The effective reduction in the *OIP3* of the serial array as a function of the position of the "bad" NLE is

$$\chi_{eff}(\sigma) \equiv \frac{OIP3_{ser,1-bad}(\sigma)}{OIP3_{ser,ident}}, \tag{22}$$

where $OIP3_{ser,1-bad}(\sigma)$ is due to one "bad" NLE and $OIP3_{ser,ident}$ corresponds to all identical, "good" NLEs. Both *OIP3* values are obtained from (14) and (15) for the coherent and incoherent cases, respectively.

Since $OIP3_{ser,1-bad}(\sigma)$ depends on the location of the "bad" NLE, we have found it advantageous to write three different expressions for $\chi_{eff}(\sigma)$. Each expression corresponds to one of three regimes: $\sigma = 1$, $1 < \sigma < S$, and $\sigma = S$. For the coherent case,

$$\chi_{eff,coh}(\sigma = 1) = \frac{\left[1+\frac{1}{\chi G^{(S-1)}}+\frac{1}{G^{(S-2)}}\left(\frac{G^{(S-2)}-1}{G-1}\right)\right]^{-1}}{\left[1+\frac{1}{G^{(S-1)}}\left(\frac{G^{(S-1)}-1}{G-1}\right)\right]^{-1}}, \tag{23}$$

$$\chi_{eff,coh}(1 < \sigma < S) = \frac{\left[1+\frac{1}{\gamma G^{(S-1)}}\left(\frac{G^{(\sigma-1)}-1}{G-1}\right)+\frac{1}{\chi G^{(S-\sigma)}}+\frac{1}{G^{(S-1)}}\left(\frac{G^{(S-1)}-G^{\sigma}}{G-1}\right)\right]^{-1}}{\left[1+\frac{1}{G^{(S-1)}}\left(\frac{G^{(S-1)}-1}{G-1}\right)\right]^{-1}}, \tag{24}$$

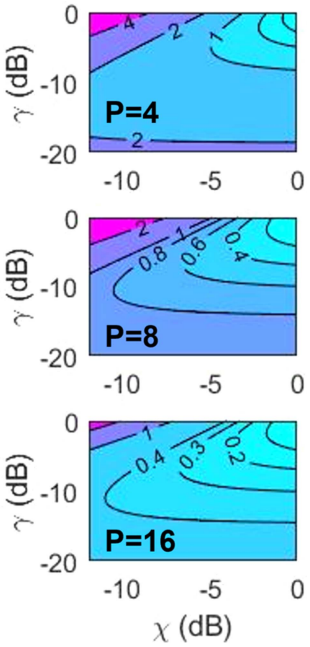

FIGURE 4. Contour plots of the reduction (dB) in the coherent *OIP3* of a parallel array, $R_{1-bad,coh}$, due to the presence of one "bad" NLE amongst otherwise identical, "good" NLEs for $S = 1$ and $P = 4$, 8, & 16. The reduction depends on channel count P, as well as the degree of degradation of the RF power gain and *OIP3* of the "bad" NLE, which are quantified by $\gamma(dB)$ and $\chi(dB)$, respectively, but is independent of the position ρ of the "bad" element, confirming the analysis in this section for a system containing one "bad" NLE.

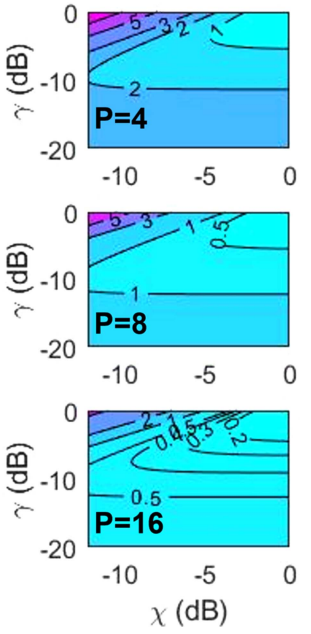

FIGURE 5. Contour plots of the reduction (dB) in the incoherent *OIP3* of a parallel array, $R_{1-bad,incoh}$, due to the presence of one "bad" NLE amongst otherwise identical, "good" NLEs for $S = 1$ and $P = 4$, 8, & 16. The reduction depends on channel count P, as well as the degree of degradation of the RF power gain and *OIP3* of the "bad" NLE, which are quantified by $\gamma(dB)$ and $\chi(dB)$, respectively, but is independent of the position ρ of the "bad" element, confirming the analysis in this section for a system containing one "bad" NLE.

$$\chi_{eff,coh}(\sigma = S) = \frac{\left[\frac{1}{\chi} + \frac{1}{G^{(S-1)}}\left(\frac{G^{(S-1)}-1}{G-1}\right)\right]^{-1}}{\left[1 + \frac{1}{G^{(S-1)}}\left(\frac{G^{(S-1)}-1}{G-1}\right)\right]^{-1}}. \tag{25}$$

For the incoherent case we find

$$\chi_{eff,incoh}(\sigma = 1) = \frac{\left[1 + \frac{1}{\chi^2 G^{2(S-1)}} + \frac{1}{G^{2(S-2)}}\left(\frac{G^{2(S-2)}-1}{G^2-1}\right)\right]^{-\frac{1}{2}}}{\left[1 + \frac{1}{G^{2(S-1)}}\left(\frac{G^{2(S-1)}-1}{G^2-1}\right)\right]^{-\frac{1}{2}}}, \tag{26}$$

$$\chi_{eff,incoh}(1 < \sigma < S) = \frac{\left[1 + \frac{1}{\gamma^2 G^{2(S-1)}}\left(\frac{G^{2(\sigma-1)}-1}{G^2-1}\right) + \frac{1}{\chi^2 G^{2(S-\sigma)}} + \frac{1}{G^{2(S-1)}}\left(\frac{G^{2(S-1)}-G^{2\sigma}}{G^2-1}\right)\right]^{-\frac{1}{2}}}{\left[1 + \frac{1}{G^{2(S-1)}}\left(\frac{G^{2(S-1)}-1}{G^2-1}\right)\right]^{-\frac{1}{2}}}, \tag{27}$$

$$\chi_{eff,incoh}(\sigma = S) = \frac{\left[\frac{1}{\chi^2} + \frac{1}{G^{2(S-1)}}\left(\frac{G^{2(S-1)}-1}{G^2-1}\right)\right]^{-\frac{1}{2}}}{\left[1 + \frac{1}{G^{2(S-1)}}\left(\frac{G^{2(S-1)}-1}{G^2-1}\right)\right]^{-\frac{1}{2}}}. \tag{28}$$

Examination of (23) through (28) reveals the following: 1) in the regimes $\sigma = 1$ and $\sigma = S$, $\chi_{eff}(\sigma)$ depends only on the degree of degradation of the *OIP3* of the "bad" NLE, χ; 2) in the regime $1 < \sigma < S$, $\chi_{eff}(\sigma)$ depends on both the degree of degradation of the RF power gain and *OIP3* of the "bad" NLE, as quantified by γ and χ, respectively; and 3) $\chi_{eff}(\sigma)$ is affected more so by χ than γ in the regime $1 < \sigma < S$.

D. FULL ARBF ARRAY: S; P = ARBITRARY; 1-BAD ELEMENT

To obtain expressions for an ARBF system containing one "bad" NLE, located at $p = \rho$ and $s = \sigma$, amongst the other identical, "good" NLEs, we combine the results from the pure parallel and pure serial arrays. The degradation in the *OIP3* of the full ARBF system is quantified by the reduction factor $R_{ARBF} \geq 1$. Using (20) and (21) for the parallel array with $\chi_{eff}(\sigma)$ in place of χ to capture the effective reduction in the *OIP3* due to the serial portion of the ARBF system, the reduction factors are, for the coherent case,

$$R_{ARBF,coh}(\sigma) \equiv \frac{OIP3_{ARBF,coh,ident}}{OIP3_{ARBF,coh,1-bad}(\sigma)} = \frac{P^2\left[(P-1) + \left(\frac{\gamma^{3/2}}{\chi_{eff,coh}(\sigma)}\right)\right]}{\left[(P-1) + \gamma^{1/2}\right]^3} \tag{29}$$

and, for the incoherent case,

$$R_{ARBF,incoh}(\sigma) \equiv \frac{OIP3_{ARBF,incoh,ident}}{OIP3_{ARBF,incoh,1-bad}(\sigma)} = \frac{P^{5/2}\left[(P-1) + \left(\frac{\gamma^3}{\chi^2_{eff,incoh}(\sigma)}\right)\right]^{1/2}}{\left[(P-1) + \gamma^{1/2}\right]^3}. \tag{30}$$

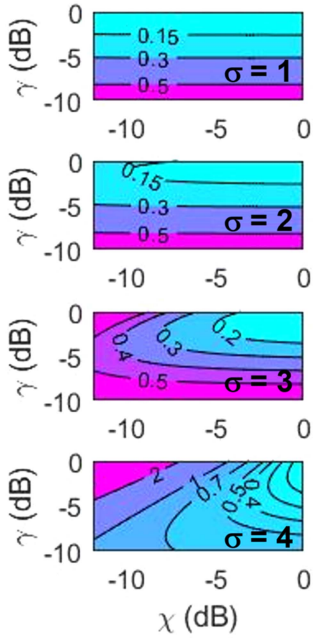

FIGURE 6. Reduction (dB) in the coherent *OIP3* of an ARBF system, $R_{ARBF,coh}(\sigma)$, due to one "bad" NLE in the presence of other identical, "good" NLEs for $S = 4$, $P = 8$, $G = 10$ dB, and $\sigma = 1, 2, 3$ & 4. The reduction depends on the stage σ containing the "bad" NLE, as well as the degree of degradation of the RF power gain and *OIP3* of the "bad" NLE, which are quantified by γ(*dB*) and χ(*dB*), respectively.

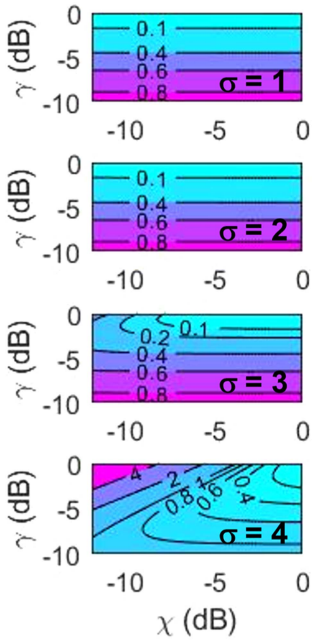

FIGURE 7. Reduction (dB) in the incoherent *OIP3* of an ARBF system, $R_{ARBF,incoh}(\sigma)$, due to one "bad" NLE in the presence of other identical, "good" NLEs for $S = 4$, $P = 8$, $G = 10$ dB, and $\sigma = 1, 2, 3$ & 4. The reduction depends on the stage σ containing the "bad" NLE, as well as the degree of degradation of the RF power gain and *OIP3* of the "bad" NLE, which are quantified by γ(*dB*) and χ(*dB*), respectively.

For the three different regimes of σ, $\chi_{eff,coh}(\sigma)$ in (29) and $\chi_{eff,incoh}(\sigma)$ in (30) are given by (23)–(25) and (26)–(28), respectively.

The reduction factors given by (29) and (30) are plotted in Figs. 6 and 7, respectively, for $S = 4$, $P = 8$, $G = 10$ dB, and $\sigma = 1, 2, 3$, and 4. Inspection of Figs. 6 and 7 shows the following: 1) the coherent case is somewhat more forgiving of one "bad" NLE; 2) the reduction is independent of the channel ρ containing the "bad" NLE and depends only on the stage σ in which the "bad" NLE is located; 3) the reduction is independent of the starting value of *OIP3* but depends on the starting value of G; and 4) the negative effect of the "bad" NLE is most significant when it is located in the last stage ($\sigma = S$).

V. EXPERIMENT

Two sets of experiments were performed using a 2 x 2 ARBF system to verify the coherent and incoherent *OIPm* expressions in Section III-B for $m = 2, 3$. The first set was conducted using all "good" NLEs with the input signal near a) 3 GHz and b) 8 GHz. The second set was done using one "bad" NLE having a significantly lower *OIPm* than the other "good" NLEs with the input signal near 3 GHz and the "bad" NLE moved to each of the four positions in the array. For these experiments we have chosen to focus on *OIP2* and *OIP3* because they are the standard metrics used to quantify multi- and single-octave linearity, respectively, in an analog RF system.

As will be seen below, the results of 36 independent measurements, representing a combination of *OIP2* and *OIP3* under various conditions, all lie within the theoretical lower (14) and upper (15) bounds, as obtained from the general result (12), once the proper experimental parameters (in Table 2 of Appendix III) are inserted. Hence, these measurements are all consistent with the theoretical analysis in Sections III and IV.

A. SETUP

For both sets of experiments, the setup in Fig. 8 was employed, which consists of a measurement system and a 2 x 2 ARBF system. The measurement system comprises signal-generation and analysis subsystems, and the 2 x 2 ARBF system comprises two channels, each containing two NLEs, and a combiner. All of the NLEs are low-noise amplifiers (LNAs).

Two electrical signal generators (ESG 1, Agilent E8251A & ESG 2, Agilent N5183A) were used to provide the input signal to the 2 x 2 ARBF system. The input signal comprised two equal-amplitude, closely-spaced, incommensurate RF tones at frequencies f_1 and f_2, $|f_2 - f_1| \ll f_1, \quad f_2$. Both signal generator outputs were bandpass filtered (BPFs 1 & 2, Reactel 7C11-3G-500 for input near 3 GHz or Reactel

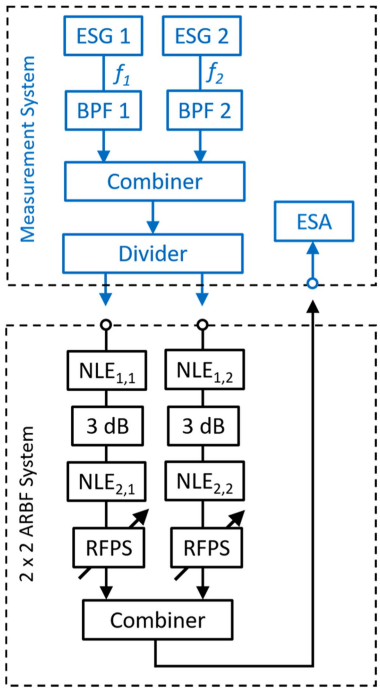

FIGURE 8. Block diagram of the experimental setup. The measurement system comprises 1) a signal-generation subsystem consisting of two electrical signal generators (ESG), two bandpass filters (BPF), an RF combiner, and an RF divider; and 2) a signal-analysis subsystem comprising an electrical spectrum analyzer (ESA). The 2 x 2 ARBF system consists of two parallel RF channels and a Wilkinson combiner. Each channel contains two nonlinear elements (NLE), a 3-dB attenuator, and an RF-phase shifter (RFPS). Relevant RF parameter values for the NLEs are summarized in Table 2 of Appendix III.

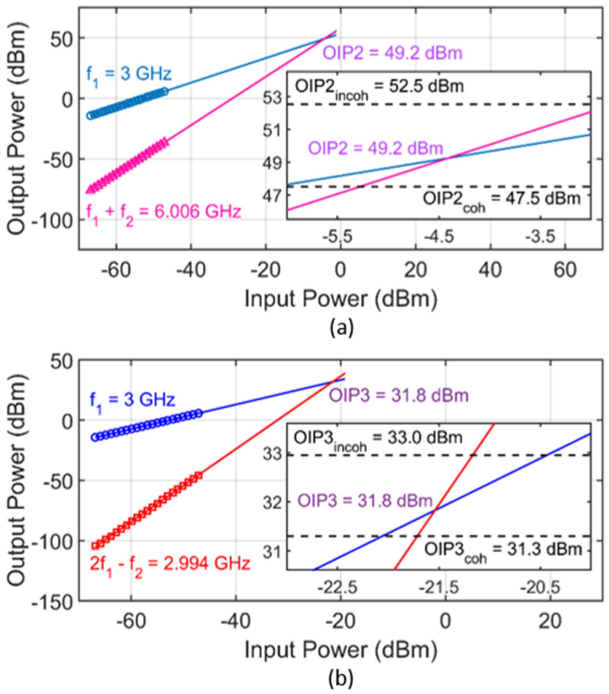

FIGURE 9. Example plots showing the *OIPm* ($m = 2, 3$) of a 2 x 2 ARBF system containing all "good" NLEs. (a) *OIP2* from small-signal responses at $f_1 = 3$ GHz and $f_1 + f_2 = 6.006$ GHz. (b) *OIP3* from small-signal responses at $f_1 = 3$ GHz and $2f_1 - f_2 = 2.994$ GHz. Shown are the measured data (symbols) and extrapolated linear fits to the measured small-signal output powers (lines), the intersection of which is the output intercept point, *OIPm*. The insets show a close-in view around the output intercept point, *OIPm*, obtained from measured data, as well as the theoretical calculated lower and upper bounds on the intercept point (dashed lines) given by $OIPm_{coh}$ and $OIPm_{incoh}$, respectively.

6C11-8G-500 for input near 8 GHz) to suppress harmonics, combined and divided with Wilkinson devices (Midwest Microwave PWD-5533-020SMA-79) having > 20 dB of isolation between input/output ports, and fed into each channel input of the ARBF system. Input power was varied over a 20 dB range in 1 dB steps with the power of both tones within 0.1 dB of one another and the input power to both channels equally balanced for all measurements. For the first set of experiments, the frequencies of the two input tones were a) 3 GHz and 3.006 GHz and b) 8 GHz and 8.006 GHz. During the second set of experiments, the two input tones were at frequencies of 3 GHz and 3.006 GHz.

In the 2 x 2 ARBF system, 3-dB attenuators were used to avoid compressing the second NLE on each channel, RF-phase shifters (RFPS 1 & 2, Sage 6705K-2) were employed to phase match the two channels, and a Wilkinson combiner (Midwest Microwave PWD-5533-02-SMA-79) was used to sum the two channel outputs. At the output of the Wilkinson combiner, the two channels were phase matched to within 5° at the frequencies of interest for the measurements. Isolation between Wilkinson combiner input ports was measured to be > 20 dB. The RF phase and isolation measurements were taken with a vector network analyzer (VNA, Agilent N5225A).

An electrical spectrum analyzer (ESA, Agilent E4440A) was used to measure the 2 x 2 ARBF system output power at the fundamental frequencies (f_1 & f_2), second-order intermodulation distortion (IMD2) sum frequency ($f_1 + f_2$), and third-order intermodulation distortion (IMD3) difference frequencies ($2f_1 - f_2$ & $2f_2 - f_1$). Each output power measurement comprised 50 log-power (video) averages. Care was taken when setting the ESA attenuation level to minimize the distortion from the ESA's frontend mixer well below the distortion being measured from the ARBF system. For all measurements, ESA IMD2 and IMD3 were ≥ 60 dB and ≥ 27 dB, respectively, below ARBF system IMD2 and IMD3.

B. RESULTS & DISCUSSION

Linear fits were applied to the ESA-measured small-signal output powers at a fundamental frequency and a distortion frequency and then extrapolated to their intersection point to yield the *OIPm* ($m = 2, 3$) of the 2 x 2 ARBF system. The theoretical lower and upper bounds on the output intercept point were calculated using the coherent and incoherent *OIPm* expressions in (14) and (15) with $m = 2$,

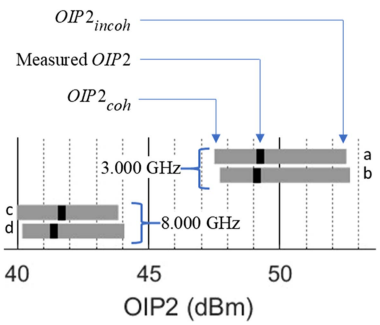

FIGURE 10. Comparing *OIP2* values for all "good" NLEs with the two-tone input near 3 GHz and 8 GHz. All measured values (black bars) occur within the gray-bar interval corresponding to the theoretical $OIP2_{coh}$ (left edge of interval) and theoretical $OIP2_{incoh}$ (right edge of interval). These *OIP2* results are for the following combinations of fundamental and IMD2 frequencies: (a) $f_1 = 3$ GHz & $f_1 + f_2 = 6.006$ GHz, (b) $f_2 = 3.006$ GHz & $f_1 + f_2 = 6.006$ GHz, (c) $f_1 = 8$ GHz & $f_1 + f_2 = 16.006$ GHz, and (d) $f_2 = 8.006$ GHz & $f_1 + f_2 = 16.006$ GHz. The device assignment for these results is as follows: $NLE_{1,1} = 116$, $NLE_{1,2} = 115$, $NLE_{2,1} = 107$, and $NLE_{2,2} = 111$. Relevant RF parameter values for these devices are contained in Table 2 of Appendix III. These values were used to calculate $OIP2_{coh}$ and $OIP2_{incoh}$.

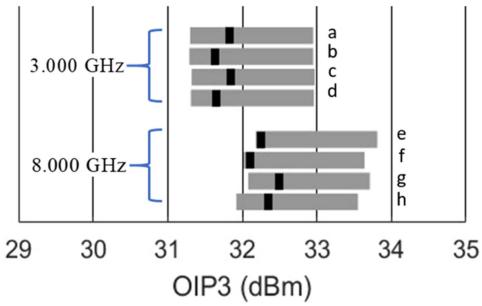

FIGURE 11. Comparing *OIP3* values for all "good" NLEs with the two-tone input near 3 GHz and 8 GHz. All measured values (black bars) occur within the gray-bar interval corresponding to the theoretical $OIP3_{coh}$ (left edge of interval) and theoretical $OIP3_{incoh}$ (right edge of interval). These *OIP3* results are for the following combinations of fundamental and IMD3 frequencies: (a) $f_1 = 3$ GHz & $2f_1 - f_2 = 2.994$ GHz, (b) $f_1 = 3$ GHz & $2f_2 - f_1 = 3.012$ GHz, (c) $f_2 = 3.006$ GHz & $2f_1 - f_2 = 2.994$ GHz, (d) $f_2 = 3.006$ GHz & $2f_2 - f_1 = 3.012$ GHz, (e) $f_1 = 8$ GHz & $2f_1 - f_2 = 7.994$ GHz, (f) $f_1 = 8$ GHz & $2f_2 - f_1 = 8.012$ GHz, (g) $f_2 = 8.006$ GHz & $2f_1 - f_2 = 7.994$ GHz, and (h) $f_2 = 8.006$ GHz & $2f_2 - f_1 = 8.012$ GHz. The device assignment for these results is as follows: $NLE_{1,1} = 116$, $NLE_{1,2} = 115$, $NLE_{2,1} = 107$, and $NLE_{2,2} = 111$. Relevant RF parameter values for these devices are contained in Table 2 of Appendix III. These values were used to calculate $OIP3_{coh}$ and $OIP3_{incoh}$.

3. Here, the calculations were done using the measured RF parameters for each channel: linear gain and *OIPm* of both NLEs, linear loss between NLEs (including cable and 3-dB attenuator losses), linear loss between the second NLE and the output (including cable and RFPS losses and the excess loss of the combiner), and the linear voltage coupling loss of the Wilkinson combiner (no intentional weighting was applied). The *OIPm* of each NLE was obtained in the same fashion as the *OIPm* of the entire ARBF system, whereas the linear gains and linear losses were measured at the fundamental and distortion frequencies with the VNA. Relevant values for these RF parameters are summarized in Table 2 of Appendix III.

Results from both sets of experiments are presented in Figs. 9–13, which show excellent agreement between theory and measurement. All measured values fall within the lower and upper bounds corresponding to the assumptions of purely coherent (14) and purely incoherent (15) distortion signals, respectively.

Fig. 9 includes example *OIPm* ($m = 2, 3$) plots for the case of a 2 x 2 ARBF system containing all "good" NLEs. *OIP2* in Fig. 9(a) is given by the intersection of the extrapolated linear fits to the measured small-signal responses at $f_1 = 3$ GHz and $f_1 + f_2 = 6.006$ GHz. Similarly, the *OIP3* in Fig. 9(b) is defined by the intersection of the extrapolated linear fits to the measured small-signal responses at $f_1 = 3$ GHz and $2f_1 - f_2 = 2.994$ GHz. On each plot, the left side shows the *OIPm* obtained from measured data, and the inset on the right side clearly shows that the *OIPm* obtained by measurement is within the theoretical calculated lower and upper bounds set by $OIPm_{coh}$ and $OIPm_{incoh}$, respectively.

Figs. 10 and 11 summarize all of the results from the first set of experiments performed with a 2 x 2 ARBF system containing all "good" NLEs. Fig. 10 shows that the *OIP2* values obtained from measured data (measured *OIP2*) are between the theoretical calculated bounds established by $OIP2_{coh}$ and $OIP2_{incoh}$. Measured *OIP2* values and the theoretical calculated bounds are reported for the two-tone input signal near a) 3 GHz and b) 8 GHz for both combinations of fundamental and IMD2 sum frequencies: f_1 & $f_1 + f_2$ and f_2 & $f_1 + f_2$. The measured *OIP2* obtained with the two-tone input near 3 GHz is significantly higher (~7.6 dB) than the *OIP2* obtained with the two-tone input near 8 GHz. Similarly, it is shown in Fig. 11 that the measured *OIP3* is within the theoretical calculated bounds given by $OIP3_{coh}$ and $OIP3_{incoh}$. Values reported here are for the two-tone input near a) 3 GHz and b) 8 GHz for all four combinations of fundamental and IMD3 difference frequencies: f_1 & $2f_1 - f_2$, f_1 & $2f_2 - f_1$, f_2 & $2f_1 - f_2$, and f_2 & $2f_2 - f_1$. The measured *OIP3* is slightly higher (~0.6 dB) for the two-tone input near 8 GHz as compared to 3 GHz.

Figs. 12 and 13 summarize all of the results from the second set of experiments conducted with one "bad" NLE in the 2 x 2 ARBF system and the two-tone input signal near 3 GHz. On the figures, the position of the "bad" NLE, $NLE_{s,p}$, is indicated by the subscripts s, p. Also shown on the figures for comparison are the results for the case of all "good" NLEs, which were obtained from the first set of experiments.

Fig. 12 shows that the measured *OIP2* is between the theoretical calculated bounds set by $OIP2_{coh}$ and $OIP2_{incoh}$. The combinations of fundamental and IMD2 frequencies at which results are reported in Fig. 12 are noted in Table 3 of Appendix III, with the assignment of devices to NLE positions also noted. In Fig. 12, the measured *OIP2* obtained with the "bad" NLE in the first stage of each channel is similar to (within 0.8 dB of) the *OIP2* for all "good" NLEs. Conversely, the measured *OIP2* obtained with the "bad" NLE in the second stage of each channel is significantly lower (~9.1 dB)

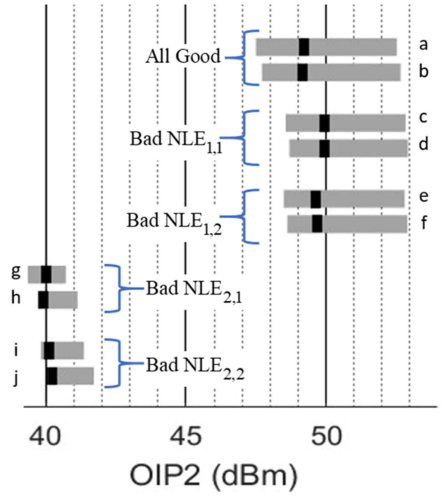

FIGURE 12. Comparing *OIP2* values obtained with the two-tone input near 3 GHz for the two cases i) all "good" NLEs (results from first set of experiments) and ii) one "bad" NLE (results from second set of experiments). Placement of the "bad" NLE is indicated by the subscripts. All measured values (black bars) are within the gray-bar intervals, whose left and right edges correspond to the theoretical $OIP2_{coh}$ and $OIP2_{incoh}$, respectively. The combinations of frequencies for *OIP2* results (a)–(j) and assignment of devices to NLE positions are summarized in Table 3 of Appendix III. Relevant RF parameter values for these devices are noted in Table 2 of Appendix III. $OIP2_{coh}$ and $OIP2_{incoh}$ were calculated using these values. Note that the *OIP2* values for "bad" $NLE_{1,1}$ and "bad" $NLE_{1,2}$ are slightly higher than the *OIP2* values for all "good" NLEs since device 114 has a substantially higher (14.1-14.6 dB) *OIP2* than device 116.

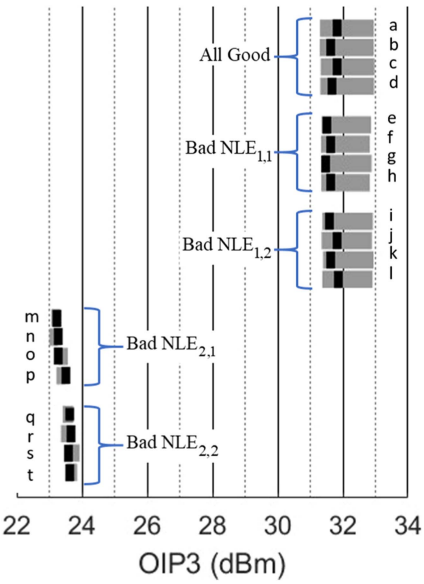

FIGURE 13. Comparing *OIP3* values obtained with the two-tone input near 3 GHz for the two cases i) all "good" NLEs (results from first set of experiments) and ii) one "bad" NLE (results from second set of experiments). Placement of the "bad" NLE is indicated by the subscripts. All measured values (black bars) are within the gray-bar intervals, whose left and right edges correspond to the theoretical $OIP3_{coh}$ and $OIP3_{incoh}$, respectively. The combinations of frequencies for *OIP3* results (a)–(t) and assignment of devices to NLE positions are summarized in Table 4 of Appendix III. Relevant RF parameter values for these devices are noted in Table 2 of Appendix III. $OIP3_{coh}$ and $OIP3_{incoh}$ were calculated using these values. Note that the *OIP3* values for "bad" $NLE_{1,1}$ and "bad" $NLE_{1,2}$ are comparable to the *OIP3* values for all "good" NLEs because device 114 has a significantly higher (10.5-11.2 dB) *OIP3* than device 116.

than the *OIP2* for all "good" NLEs. As expected from the analysis developed in Section IV-D, the channel in which the "bad" NLE is located has little bearing on the system *OIP2*.

It is shown in Fig. 13 that the measured *OIP3* is within the bounds provided by the theoretical calculated $OIP3_{coh}$ and $OIP3_{incoh}$. The results reported in Fig. 13 are for the combinations of fundamental and IMD3 difference frequencies and device assignments to NLE positions listed in Table 4 of Appendix III. From Fig. 13, the measured *OIP3* for the "bad" NLE in the first stage of each channel is similar to (within 0.4 dB of) the *OIP3* for all "good" NLEs. In contrast, the measured *OIP3* for the "bad" NLE in the second stage of each channel is substantially less (~8.3 dB) than the *OIP3* for all "good" NLEs. Unsurprisingly, the system *OIP3* is affected minimally by the channel containing the "bad" NLE but depends heavily on the stage in which the "bad" NLE resides. This finding is consistent with that from the analysis in Section IV-D.

VI. SUMMARY

In this work we obtained expressions for the *IPm* and *OIPm* of an analog receive beamforming system. The *IPm* expression was derived under the assumption that the *OIPm* and RF power gain of each individual NLE, the losses in the system, and the relative RF phase shifts at the output were all known. This general expression can be used to predict the value of an actual, measured output intercept point if all of the relevant system parameters are known. However, since the relative RF phases at each location in the array are often unknown in practice, two specific assumptions were invoked to calculate the coherent and incoherent *OIPm* values and these provide the lower and upper bounds, respectively, to any actual measured value.

Certain limiting cases of the coherent and incoherent *OIPm* for $m = 3$ were then explored. The purely parallel and purely serial arrays comprising the ARBF system were analyzed separately, then the results from these analyses were combined to provide further insight into the nonlinear behavior of the entire system. From the analysis of the parallel array, it was found that the *OIP3* of the array improves with the number of NLEs and that the effect of a "bad" NLE is independent of its location in the array and diminishes with increasing array size. Analysis of the serial array showed that the effect of a "bad" NLE depends on its location in the array. The negative impact on *OIP3* is most significant when the "bad" NLE is the last device in the chain. Unsurprisingly, the effect of the "bad" NLE on the *OIP3* of the ARBF system depends on the stage in which it is located, but not the channel, and decreases with increasing element count.

Experiments were conducted using a 2 x 2 ARBF system for two cases: 1) all "good" NLEs with the two-tone input signal near a) 3 GHz and b) 8 GHz, and 2) one "bad" NLE with its position in the array varied and the two-tone input signal near 3 GHz. For both cases, the *OIPm* ($m = 2, 3$) obtained

from measured data landed between the theoretical calculated bounds established by $OIPm_{coh}$ and $OIPm_{incoh}$. Thus, theory and measurement are in agreement.

The expressions for the *IPm* and *OIPm*, in conjunction with the findings from the limiting cases, will be of utility in the design, analysis, and testing of analog systems such as phased-arrays, multi-channel receivers, and receive-mode beamformers.

APPENDIX I

This appendix provides a summary of all the parameters used in Section III. In addition, two figures are provided that show details of various voltage amplitude and phase relationships. The parameters and their definitions are listed alphabetically in the following order for convenient reference: lowercase Roman, uppercase Roman, and lowercase Greek.

c_v = intrinsic linear voltage coupling loss of the summing junction (channel-independent),
= 1 for a lossless voltage combiner,
= $1/\sqrt{P}$ for a reactive power combiner (Wilkinson), where P is the number of combiner input ports (equal to number of channels),
= $1/P$ for a resistive power combiner;

$g_{D,sp}$ = net linear power gain at the distortion frequency between output of stage s on channel p and system output,

$$= \frac{1}{L_{D,sp}} \left(\prod_{z=s+1}^{S} \frac{G_{D,zp}}{L_{D,zp}} \right), \qquad s < S,$$

$$= \frac{1}{L_{D,Sp}}, \qquad s = S;$$

$g_{F,sp}$ = net linear power gain at the fundamental frequency between output of stage s on channel p and system output,

$$= \frac{1}{L_{F,sp}} \left(\prod_{z=s+1}^{S} \frac{G_{F,zp}}{L_{F,zp}} \right), \qquad s < S,$$

$$= \frac{1}{L_{F,Sp}}, \qquad s = S;$$

p = an index that labels the channel in a parallel array of P channels;

$p_{D,tot}$ = total mth-order distortion power from all S stages and P channels at system output;

$p_{F,tot}$ = total fundamental power from all P channels at system output;

s = an index that labels the stage in a serial cascaded of S stages;

$v_{D,sp}$ = mth-order distortion voltage phasor at system output that originated in stage s on channel p,
$= V_{D,sp}\sqrt{g_{D,sp}}\alpha_p e^{i(\varphi_{sp}+\gamma_p)}$,
$= D_{sp}e^{i\xi_{sp}}$;

$v_{F,p}$ = fundamental voltage phasor from channel p at system output,
$= V_{F,Sp}\alpha_p e^{i(\chi_p+\psi_p)}$,
$= F_{Sp}e^{i(\chi_p+\psi_p)}$,
$= v_{F,sp}$;

$v_{F,sp}$ = fundamental voltage phasor at output of stage s, channel p referred to system output,
$= V_{F,sp}\sqrt{g_{F,sp}}\alpha_p e^{i(\chi_p+\psi_p)}$,
$= F_{sp}e^{i(\chi_p+\psi_p)}$;

w_p = intentionally applied voltage weighting (linear loss) on channel p, where $0 \le w_p \le 1$ (intentional channel weighting is typically applied in a receive-mode beamformer to minimize sidelobe levels);

$D_{sp} = V_{D,sp}\sqrt{g_{D,sp}}\alpha_p$;

$F_{sp} = V_{F,sp}\sqrt{g_{F,sp}}\alpha_p$;

$F_{Sp} = V_{F,Sp}\alpha_p$;

$G_{D,sp}$ = linear power gain of stage s on channel p at the distortion frequency, where $G_{D,sp} > 0$ (accounts for NLEs with $<$ or $\ge$ unity gain, as would be the case for an RF mixer or amplifier, respectively);

$G_{F,sp}$ = linear power gain of stage s on channel p at the fundamental frequency, where $G_{F,sp} > 0$ (accounts for NLEs with $<$ or $\ge$ unity gain, as would be the case for an RF mixer or amplifier, respectively);

$L_{D,sp}$ = linear power loss in between stage s and stage $s+1$ on channel p at the distortion frequency (also encompasses loss in between final stage S and the system output, which includes excess loss, but not coupling loss, of the summing junction), where $L_{D,sp} \ge 1$;

$L_{F,sp}$ = linear power loss in between stage s and stage $s+1$ on channel p at the fundamental frequency (also encompasses loss in between final stage S and the system output, which includes excess loss, but not coupling loss, of the summing junction), where $L_{F,sp} \ge 1$;

$OIPm_{sp}$ = mth-order output intercept point of stage s on channel p;

V_0 = amplitude of either voltage phasor input to channel p (same on all P channels);

$V_{D,sp}$ = amplitude of distortion voltage phasor at output of stage s, channel p that originated in stage s, channel p due entirely to the amplitude of the fundamental voltage at the input to stage s on channel p,

$$= V_0^m \left(\prod_{l=1}^{s-1} \frac{G_{F,lp}^{m/2}}{L_{F,lp}^{m/2}} \right) \frac{G_{F,sp}^{m/2}}{OIPm_{sp}^{(m-1)/2}(2Z_0)^{(m-1)/2}}, \qquad s > 1,$$

$$= V_0^m \frac{G_{F,1p}^{m/2}}{OIPm_{1p}^{(m-1)/2}(2Z_0)^{(m-1)/2}}, \qquad s = 1;$$

$V_{F,sp}$ = amplitude of fundamental voltage phasor at output of stage s, channel p,

$$= V_0 \left(\prod_{l=1}^{s-1} \frac{G_{F,lp}^{1/2}}{L_{F,lp}^{1/2}} \right) G_{F,sp}^{1/2}, \qquad s > 1,$$

$$= V_0 G_{F,1p}^{1/2}, \qquad s = 1;$$

$V_{F,Sp}$ = amplitude of fundamental voltage phasor from channel p at system output,

$$= V_0\left(\prod_{s=1}^{S}\frac{G_{F,sp}^{1/2}}{L_{F,sp}^{1/2}}\right);$$

Z_0 = output load resistance, which is assumed to be matched to the source resistance, as well as the input and output resistances of all S stages on all P channels;

α_p = voltage amplitude weighting factor on channel p (frequency-independent),
$= w_p c_v$;

γ_p = relative phase at distortion frequency between channel p and channel 1 at system output due to phase imbalances between channels, not distortion itself,
$= \gamma_p^{'} - \gamma_1^{'}$;

$\gamma_p^{'}$ = absolute phase accumulated by distortion from all S stages on channel p between o/p A and system output (o/p A: reference plane between output of final stage S and combiner input on all P channels, see Fig. 15);

$\gamma_{p,q} = \gamma_p - \gamma_q$;

θ_{sp} = absolute phase accumulated by distortion originating in stage s, channel p between stage output and o/p A;

$\xi_{sp} = \varphi_{sp} + \gamma_p$;

$\xi_{sp,rp} = \xi_{sp} - \xi_{rp} = \varphi_{sp,rp}$;

$\xi_{sp,rq} = \xi_{sp} - \xi_{rq} = \varphi_{sp,rq} + \gamma_{p,q}$;

$\xi_{sp,sq} = \xi_{sp} - \xi_{sq} = \varphi_{sp,sq} + \gamma_{p,q}$;

ϕ_{sp} = absolute initial phase of distortion originating in stage s, channel p as measured at stage output;

φ_{sp} = absolute phase of distortion originating in stage s, channel p at o/p A (see Fig. 15),
$= \phi_{sp} + \theta_{sp}$;

$\varphi_{sp,rp} = \varphi_{sp} - \varphi_{rp}$;

$\varphi_{sp,rq} = \varphi_{sp} - \varphi_{rq}$;

$\varphi_{sp,sq} = \varphi_{sp} - \varphi_{sq}$;

χ_p = relative phase at fundamental frequency between channel p and channel 1 at o/p A due to phase imbalances between channels,
$= \chi_p^{'} - \chi_1^{'}$;

$\chi_p + \psi_p$ = relative phase at fundamental frequency between channel p and channel 1 at system output due to phase imbalances between channels;

$\chi_p^{'}$ = absolute phase accumulated by fundamental on channel p between input p and o/p A (see Fig. 15);

ψ_p = relative phase imbalance between channel p and channel 1 at the fundamental frequency that occurs between o/p A and the system output,
$= \psi_p^{'} - \psi_1^{'}$;

$\psi_{p,q} = \psi_p - \psi_q$;

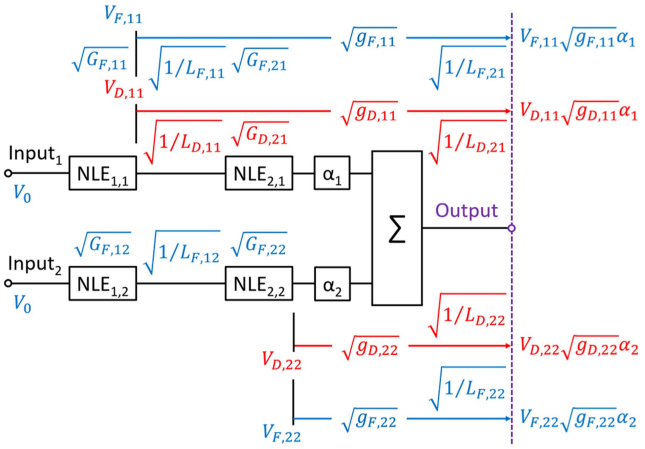

FIGURE 14. Diagram for a two-stage, two-channel ARBF system showing channel input voltage phasor amplitudes, net linear voltage gains, voltage amplitude weighting, and voltage phasor amplitudes out of NLE$_{1,1}$ and NLE$_{2,2}$ at the system output (fundamental: blue, distortion: red). From the output of NLE$_{1,1}$ to the system output, the net linear voltage gain includes the linear voltage loss between NLE$_{1,1}$ and NLE$_{2,1}$, the linear voltage gain of NLE$_{2,1}$, and the linear voltage loss between NLE$_{2,1}$ and the system output. From the output of NLE$_{2,2}$ to the system output, the net linear voltage gain contains only the linear voltage loss between NLE$_{2,2}$ and the system output. Voltage amplitude weighting includes coupling loss of the summing junction and intentionally applied loss.

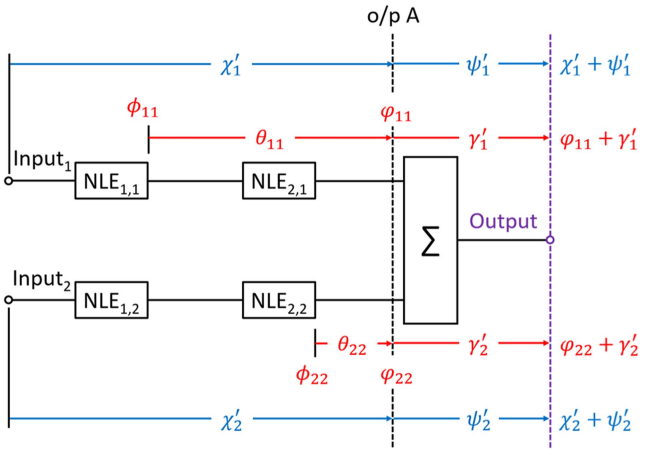

FIGURE 15. Diagram for a two-stage, two-channel ARBF system showing absolute phases of the channel input voltages and distortion voltages out of NLE$_{1,1}$ and NLE$_{2,2}$ at the system output (fundamental: blue, distortion: red), which are associated with the respective voltage phasor amplitudes shown in Fig. 14. The absolute phase of the fundamental at the system output consists of the phase accumulated between the channel input and o/p A and the phase accumulated between o/p A and the system output. The absolute phase of the distortion at the system output comprises the initial phase of the distortion at the stage output, the phase accumulated between the stage output and o/p A, and the phase accumulated between o/p A and the system output.

$\psi_p^{'}$ = absolute phase accumulated by fundamental on channel p between o/p A and system output (see Fig. 15).

To supplement the definitions, Figs. 14 and 15 illustrate the relationships among some of the parameters for the special case $S = P = 2$. Fig. 14 shows the voltage phasor amplitudes,

linear voltage gains, linear voltage losses, and voltage weighting factors. The voltage phasor amplitudes at the system output are associated with the fundamental and distortion voltage phasor amplitudes at the outputs of $NLE_{1,1}$ and $NLE_{2,2}$. Recall that the fundamental voltage phasor amplitude at the output of the stage under consideration is expressed in terms of the channel input voltage phasor amplitude V_0. Fig. 15 shows the absolute phases. The distortion phases at the system output are related to the distortion voltage phasor amplitudes at the outputs of $NLE_{1,1}$ and $NLE_{2,2}$. The fundamental phases at the system output are associated with the channel input voltage phasor amplitude V_0.

APPENDIX II

The below identities are useful in Sections III and IV.

A. SUMMATIONS

$$\sum_p X_p^2 + \sum_{p\neq q} X_p X_q = \left(\sum_p X_p\right)^2 \tag{31}$$

$$\sum_p X_{sp}^2 + \sum_{p\neq q} X_{sp} X_{sq} = \left(\sum_p X_{sp}\right)^2 \tag{32}$$

$$\sum_s \frac{N_s^2}{\left(M_s^2\right)^3} + \sum_{s\neq r} \frac{N_s N_r}{(M_s M_r)^3} = \left(\sum_s \frac{N_s}{M_s^3}\right)^2 \tag{33}$$

$$\sum_p X_{sp} X_{rp} + \sum_{p\neq q} X_{sp} X_{rq} = \sum_{p,q} X_{sp} X_{rq} \tag{34}$$

where X, N, and M are all real.

B. GEOMETRIC SERIES

$$\sum_{s=0}^{S-1} x^s = \frac{x^S - 1}{x - 1} \qquad |x| \neq 1 \tag{35}$$

$$\sum_{s=1}^{S} x^s = \frac{x^{(S+1)} - 1}{x - 1} - 1 \qquad |x| \neq 1 \tag{36}$$

APPENDIX III

Below are tables that supplement the figures in Section V.

Table 2 contains relevant RF parameter values for the devices (LNAs) assigned to NLE positions in the 2 x 2 ARBF system of Fig. 8. Devices are identified by number in the table. All parameter values are a function of frequency and are provided for the two-tone input signal at a) $f_1 = 3$ GHz & $f_2 = 3.006$ GHz and b) $f_1 = 8$ GHz & $f_2 = 8.006$ GHz. The linear gains G (dB) and output intercept points $OIP2$ (dBm) and $OIP3$ (dBm) are noted for each NLE. The linear loss L (dB) corresponds to the NLE preceding the loss and accounts for 1) the loss between NLEs and 2) the loss between the second NLE and the system output. These linear gains, linear losses, and output intercept points, along with the $1/\sqrt{2}$ voltage coupling loss of the Wilkinson combiner, were inserted into (14) and (15) to compute the coherent and incoherent $OIPm$.

TABLE 2. RF Parameter Values for Devices in 2 x 2 ARBF System of Fig. 8

	Parameter	Device #				
		107	111	114	115	116
f_1 = 3.000 GHz f_2 = 3.006 GHz	$G(f_1)$	27.5	28.8	28.5	28.4	29.4
	$G(f_2)$	27.5	28.8	28.6	28.4	29.4
	$G(f_1+f_2)$	29.1	29.9	na	29.0	na
	$G(2f_1-f_2)$	27.5	28.7	na	28.3	na
	$G(2f_2-f_1)$	27.5	28.8	na	28.4	na
	$OIP2(f_1 \& f_1+f_2)$	46.7	48.0	47.6	33.3	33.0
	$OIP2(f_2 \& f_1+f_2)$	46.8	48.1	47.8	33.7	33.7
	$OIP3(f_1 \& 2f_1-f_2)$	28.9	29.4	29.2	18.8	18.3
	$OIP3(f_1 \& 2f_2-f_1)$	29.0	29.3	29.3	18.8	18.1
	$OIP3(f_2 \& 2f_1-f_2)$	28.9	29.4	29.3	19.1	18.8
	$OIP3(f_2 \& 2f_2-f_1)$	29.0	29.3	29.5	19.0	18.5
	$L(f_1)$	0.7	0.7	3.1	3.1	3.0
	$L(f_2)$	0.7	0.7	3.1	3.1	3.0
	$L(f_1+f_2)$	1.0	1.1	3.2	3.2	3.2
	$L(2f_1-f_2)$	0.7	0.7	3.1	3.1	3.0
	$L(2f_2-f_1)$	0.7	0.7	3.1	3.1	3.0
f_1 = 8.000 GHz f_2 = 8.006 GHz	$G(f_1)$	28.7	29.7	na	28.0	28.9
	$G(f_2)$	28.7	29.7	na	27.9	28.8
	$G(f_1+f_2)$	28.9	29.2	na	na	na
	$G(2f_1-f_2)$	28.7	29.7	na	na	na
	$G(2f_2-f_1)$	28.7	29.7	na	na	na
	$OIP2(f_1 \& f_1+f_2)$	38.8	38.4	na	31.7	31.2
	$OIP2(f_2 \& f_1+f_2)$	38.9	38.6	na	31.6	31.3
	$OIP3(f_1 \& 2f_1-f_2)$	30.6	30.6	na	21.2	19.1
	$OIP3(f_1 \& 2f_2-f_1)$	30.5	30.4	na	21.4	19.2
	$OIP3(f_2 \& 2f_1-f_2)$	30.3	30.6	na	21.1	19.1
	$OIP3(f_2 \& 2f_2-f_1)$	30.3	30.4	na	21.3	19.1
	$L(f_1)$	1.3	1.3	na	3.2	3.2
	$L(f_2)$	1.2	1.3	na	3.3	3.3
	$L(f_1+f_2)$	1.9	2.0	na	3.2	3.5
	$L(2f_1-f_2)$	1.3	1.4	na	3.2	3.2
	$L(2f_2-f_1)$	1.2	1.3	na	3.3	3.3

Table 3 includes the combinations of frequencies and assignment of devices to NLE positions in the 2 x 2 ARBF system for $OIP2$ results (a)–(j) in Fig. 12. Frequency combinations are noted in the "Freqs" column of the table. RF parameter values for the devices are found in Table 2.

Table 4 summarizes the combinations of frequencies and assignment of devices to NLE positions in the 2 x 2 ARBF system for $OIP3$ results (a)–(t) in Fig. 13. Frequency combinations and parameter values are found as in Table 3.

TABLE 3. Frequencies and Assignment of Devices for *OIP2* Results in Fig. 12

	Freqs	$NLE_{1,1}$	$NLE_{1,2}$	$NLE_{2,1}$	$NLE_{2,2}$
a	f_1 & f_1+f_2	116	115	107	111
b	f_2 & f_1+f_2	116	115	107	111
c	f_1 & f_1+f_2	115	114	107	111
d	f_2 & f_2+f_1	115	114	107	111
e	f_1 & f_1+f_2	114	115	107	111
f	f_2 & f_1+f_2	114	115	107	111
g	f_1 & f_1+f_2	111	114	115	107
h	f_2 & f_1+f_2	111	114	115	107
i	f_1 & f_1+f_2	111	114	107	115
j	f_2 & f_1+f_2	111	114	107	115

TABLE 4. Frequencies and Assignment of Devices for *OIP3* Results in Fig. 13

	Freqs	$NLE_{1,1}$	$NLE_{1,2}$	$NLE_{2,1}$	$NLE_{2,2}$
a	f_1 & $2f_1-f_2$	116	115	107	111
b	f_1 & $2f_2-f_1$	116	115	107	111
c	f_2 & $2f_1-f_2$	116	115	107	111
d	f_2 & $2f_2-f_1$	116	115	107	111
e	f_1 & $2f_1-f_2$	115	114	107	111
f	f_1 & $2f_2-f_1$	115	114	107	111
g	f_2 & $2f_1-f_2$	115	114	107	111
h	f_2 & $2f_2-f_1$	115	114	107	111
i	f_1 & $2f_1-f_2$	114	115	107	111
j	f_1 & $2f_2-f_1$	114	115	107	111
k	f_2 & $2f_1-f_2$	114	115	107	111
l	f_2 & $2f_2-f_1$	114	115	107	111
m	f_1 & $2f_1-f_2$	111	114	115	107
n	f_1 & $2f_2-f_1$	111	114	115	107
o	f_2 & $2f_1-f_2$	111	114	115	107
p	f_2 & $2f_2-f_1$	111	114	115	107
q	f_1 & $2f_1-f_2$	111	114	107	115
r	f_1 & $2f_2-f_1$	111	114	107	115
s	f_2 & $2f_1-f_2$	111	114	107	115
t	f_2 & $2f_2-f_1$	111	114	107	115

REFERENCES

[1] T. M. Comberiate, S. H. Talisa, and K. W. O'Haver, "A comparison of in-band linearity between element-digital arrays and active electronically-steered arrays," in *Proc. IEEE Int. Symp. Phased Array Syst. Technol.*, 2016, pp. 1–4.

[2] N. Peccarelli, B. James, R. Irazoqui, J. Metcalf, C. Fulton, and M. Yeary, "Survey: Characterization and mitigation of spatial/spectral interferers and transceiver nonlinearities for 5G MIMO systems," *IEEE Trans. Microw. Theory Techn.*, vol. 67, no. 7, pp. 2829–2846, Jul. 2019.

[3] D. I. Lialios, C. L. Zekios, S. V. Georgakopoulos, and G. A. Kyriacou, "A novel RF to millimeter waves frequency translation scheme for ultra-wideband beamformers supporting the Sub-6 GHz band," *IEEE Trans. Antennas Propag.*, vol. 70, no. 12, pp. 11718–11733, Dec. 2022.

[4] H. Krishnaswamy and L. Zhang, "Analog and RF interference mitigation for integrated MIMO receive arrays," *Proc. IEEE*, vol. 104, no. 3, pp. 561–575, Mar. 2016.

[5] E. H. Mujammami, I. Afifi, and A. B. Sebak, "Optimum wideband high gain analog beamforming network for 5G applications," *IEEE Access*, vol. 7, pp. 52226–52237, 2019.

[6] M. L. G. Heras et al., "CROWN project, towards a European multifunction AESA system," in *Proc. IEEE Int. Symp. Phased Array Syst. Technol.*, 2022, pp. 1–8.

[7] D. M. Pozar, *Microwave Engineering*, 4th ed. Hoboken, NJ, USA: Wiley, 2012.

[8] N. G. Kanaglekar, R. E. McIntosh, and W. E. Bryant, "Analysis of two-tone, third-order distortion in cascaded two-ports," *IEEE Trans. Microw. Theory Techn.*, vol. 36, no. 4, pp. 701–705, Apr. 1988.

[9] S. A. Maas, *Nonlinear Microwave and RF Circuits*, 2nd ed. Norwood, MA, USA: Artech House, 2003.

[10] S. E. Wilson, "Evaluate the distortion of modular cascades," *Microwaves*, pp. 67–70, Mar. 1981.

[11] B. Rupakula and G. M. Rebeiz, "Third-order intermodulation effects and system sensitivity degradation in receive-mode 5G phased arrays in the presence of multiple interferers," *IEEE Trans. Microw. Theory Techn.*, vol. 66, no. 12, pp. 5780–5795, Dec. 2018.

[12] R. V. Gatti, M. Dionigi, and R. Sorrentino, "Computation of gain, noise figure, and third-order intercept of active array antennas," *IEEE Trans. Antennas Propag.*, vol. 52, no. 11, pp. 3139–3142, Nov. 2004.

[13] E. L. Holzman, "Intercept points of active phased array antennas," in *Proc. IEEE MTT-S Int. Microw. Symp.*, 1996, vol. 2, pp. 999–1002.

[14] F. Bucholtz, M. J. Mondich, and J. M. Singley, "Distortion metrics for multiple-input, single-output systems in terms of nonlinear polynomial coefficients," NRL Memorandum Rep. NRL/5650/MR—2023/1, Jan. 2023.

[15] A. Navarrini et al., "A 2.3-8.2 GHz room temperature multi-channel receiver for phased array feed application," in *Proc. IEEE 2nd Ukraine Conf. Elect. Comput. Eng.*, 2019, pp. 144–148.

[16] X. Chen, X. Ye, C. Wang, A. Hu, and J. Miao, "A Ka band multi-channel integrated receiver for passive millimeter wave imaging system," in *Proc. Prog. Electromagn. Res. Symp.*, 2018, pp. 2099–2105.

[17] K. Spoof, V. Unnikrishnan, M. Zahra, K. Stadius, M. Kosunen, and J. Ryynänen, "True-time-delay beamforming receiver with RF resampling," *IEEE Trans. Circuits Syst. I, Reg. Papers*, vol. 67, no. 12, pp. 4457–4469, Dec. 2020.

[18] M. J. Mondich, J. D. McKinney, F. Bucholtz, J. M. Singley, I. M. Maize, and K. J. Williams, "Group delay-based wideband photonic receive-mode radio-frequency beamforming," *J. Lightw. Technol.*, vol. 38, no. 21, pp. 5893–5907, Nov. 2020.